This paper is available online at www.jbc.org

THE JOURNAL OF BIOLOGICAL CHEMISTRY VOL. 285, NO. 45, pp. 34304–34308, November 5, 2010

Zinc Dyshomeostasis Is Linked with the Loss of Mucolipidosis IV-associated TRPML1 Ion Channel*[S]

Received for publication, July 16, 2010, and in revised form, September 9, 2010
Published, JBC Papers in Press, September 23, 2010, DOI 10.1074/jbc.C110.165480

Jonathan L. Eichelsdoerfer[‡1], Jeffrey A. Evans[‡1], Susan A. Slaugenhaupt[§], and Math P. Cuajungco[‡¶2]

From the [‡]Department of Biological Science and Center for Applied Biotechnology Studies, California State University, Fullerton, California 92831, the [§]Department of Neurology, Massachusetts General Hospital and Harvard Medical School, Boston, Massachusetts 02115, and the [¶]Mental Health Research Institute, Parkville, 3052 Victoria, Australia

Chelatable zinc is important in brain function, and its homeostasis is maintained to prevent cytotoxic overload. However, certain pathologic events result in intracellular zinc accumulation in lysosomes and mitochondria. Abnormal lysosomes and mitochondria are common features of the human lysosomal storage disorder known as mucolipidosis IV (MLIV). MLIV is caused by the loss of TRPML1 ion channel function. MLIV cells develop large hyperacidic lysosomes, membranous vacuoles, mitochondrial fragmentation, and autophagic dysfunction. Here, we observed that RNA interference of mucolipin-1 gene (TRPML1) in HEK-293 cells mimics the MLIV cell phenotype consisting of large lysosomes and membranous vacuoles that accumulate chelatable zinc. To show that abnormal chelatable zinc levels are indeed correlated with MLIV pathology, we quantified its concentration in cultured MLIV patient fibroblast and control cells with a spectrofluorometer using *N*-(6-methoxy-8-quinolyl)-*p*-toluene sulfonamide fluorochrome. We found a significant increase of chelatable zinc levels in MLIV cells but not in control cells. Furthermore, we quantified various metal isotopes in whole brain tissue of TRPML1$^{-/-}$ null mice and wild-type littermates using inductively coupled plasma mass spectrometry and observed that the zinc-66 isotope is markedly elevated in the brain of TRPML1$^{-/-}$ mice when compared with controls. In conclusion, we show for the first time that the loss of TRPML1 function results in intracellular chelatable zinc dyshomeostasis. We propose that chelatable zinc accumulation in large lysosomes and membranous vacuoles may contribute to the pathogenesis of the disease and progressive cell degeneration in MLIV patients.

Zinc (Zn^{2+}) is a redox-inert yet crucial trace element for virtually all organisms. Zn^{2+} is second to iron in biological trace metal abundance and is known to play an important role in human brain function (1, 2). Some enzymes require Zn^{2+} as co-factors, but many proteins use it for structural stability and thus are tightly bound (non-chelatable form) (3). A chelatable pool of Zn^{2+} is present in cells, most notably in glutamatergic vesicles, and gets released at the neuronal synapse during normal and pathological states (4, 5). Because high levels of chelatable Zn^{2+} or any trace metals produce cellular and mitochondrial toxicity (1, 6, 7), it is imperative that Zn^{2+} homeostasis is actively maintained inside and outside of the cells. Certain pathological events such as epilepsy, cerebral stroke, and traumatic brain injury result in uncontrolled release and accumulation of chelatable Zn^{2+} in neurons (1, 8) via voltage-gated or calcium-permeable ion channels (9). Furthermore, endosomes, autophagosomes, and lysosomes, which are critical organelles involved in the recycling and degradation of many proteins, are known compartments where chelatable Zn^{2+} accumulates upon cellular perturbation (10–12). Interestingly, chelatable Zn^{2+} appears to mediate vacuolar formation in primary retinal cells exposed to ethambutol (an antituberculosis drug known for its ocular toxicity) (13, 14) and autophagic vacuole formation in astrocytes upon exposure to hydrogen peroxide (12). Consequently, high levels of chelatable Zn^{2+} accrue in ethambutol-induced vacuoles, which induce lysosomal membrane permeabilization and retinal cell death (13). The association of chelatable Zn^{2+} in neurodegeneration led us to study its potential role in mucolipidosis IV (MLIV),[3] a developmental disorder that results in large hyperacidic lysosomes, membranous vacuole formation, autophagic dysfunction, and mitochondrial fragmentation (15–18). MLIV is an autosomal, recessive disease that generally results in brain and cognitive dysfunction, corneal clouding, and retinal cell degeneration leading to blindness, anemia, and achlorhydria (lack of gastric acid production in the stomach) (19). It is caused by the loss of transient receptor potential mucolipin-1 (TRPML1) ion channel function. TRPML1 is widely expressed in tissues and organs. It is a lysosomal membrane protein believed to play a role in endosomal-lysosomal interaction, lysosomal pH stability, lysosome maturation, lipid metabolism, and autophagy (16–18, 20, 21). TRPML1 is an inwardly rectifying, non-selective cation channel that is permeable to calcium (Ca^{2+}) and other divalent trace metals such as Zn^{2+}, iron (Fe^{2+}), and manganese (Mn^{2+}) (22–24). It is noteworthy that histochemical Prussian blue staining shows that chelatable Fe^{2+} levels in the cytosol of MLIV fibroblasts appear to be reduced, whereas levels in the lysosomes appear elevated when compared with control cells (22). These findings suggest that an impairment in chelatable Fe^{2+} permeability may be causal to MLIV disease (22). Notwithstanding, we hypothesize that chelatable Zn^{2+}, and not Fe^{2+}, could be the

* This work was supported, in whole or in part, by National Institutes of Health Grant R01 NS39995 (to S. A. S.). This work was also partially supported by Doris Howell-CSUPERB research scholarships (to J. L. E. and J. A. E.), the Howard Hughes Medical Institute undergraduate research program, and National Science Foundation Grant MCB 920127 (to M. P. C.). A preliminary account of this work was presented in the Experimental Biology 2010 meeting on April 26, 2010 in Anaheim, CA.

[S] The on-line version of this article (available at http://www.jbc.org) contains supplemental Figs. S1 and S2.

[1] Both authors contributed equally to this work.

[2] To whom correspondence should be addressed: Dept. of Biological Science, California State University, 800 N. State College Blvd., Fullerton, CA 92831. Tel.: 657-278-8522; Fax: 657-278-3426; E-mail: mcuajungco@fullerton.edu.

[3] The abbreviations used are: MLIV, mucolipidosis IV; ICP-MS, inductively coupled plasma mass spectrometry; TSQ, *N*-(6-methoxy-8-quinolyl)-*p*-toluene sulfonamide.

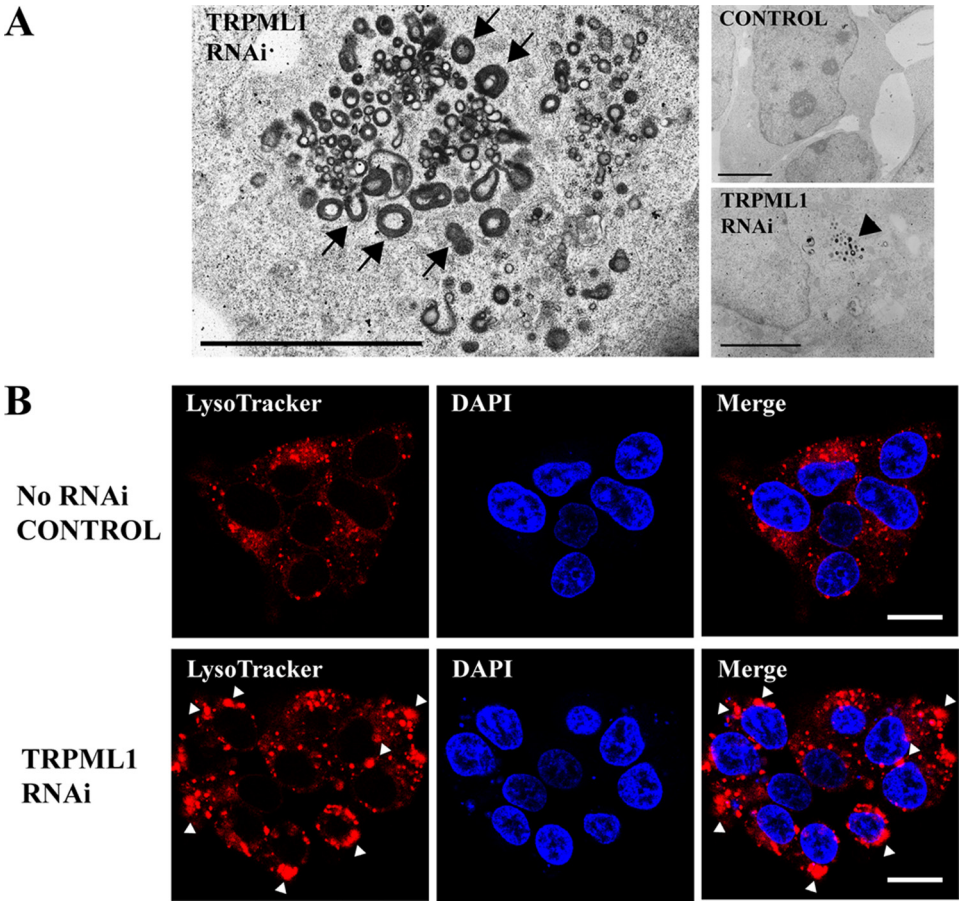

FIGURE 1. **Electron and confocal micrographs of TRPML1 RNAi-treated and control HEK-293 cells.** *A*, representative electron micrographs of TRPML1 RNAi-treated cells show electron-dense, membranous vacuoles and inclusion bodies (*right panel*, *arrow*) when compared with control. Phagophore-like structures exemplified by half-circle or horseshoe-shaped membranes can be seen near vacuolar organelles (*arrowheads*). *Scale bar* = 1 μm. *B*, representative confocal micrographs showing untreated control (*top panel*) and TRPML1 RNAi-treated HEK-293 cells (*bottom panel*). Lysosomes (*red*) are positive for LysoTracker fluorescence in control and RNAi-treated cells; however, a marked number of large lysosomal structures are only observed in TRPML1 RNAi-treated cells. Enlarged and hyperacidic lysosomes in cells are phenotypic features of ML-IV pathology. The cell nucleus (*blue*) was stained with DAPI. Scale bar = 10 μm.

mitigating factor in the cellular pathology and progressive cell degeneration in MLIV disease. In this report, we investigated whether chelatable Zn^{2+} invariably accumulates within lysosomes of cells following RNA interference of TRPML1 and whether its concentrations are significantly perturbed upon the loss of TRPML1 ion channel function in MLIV patient fibroblast cells, as well as in the brain tissue of TRPML1$^{-/-}$ knockout mice.

EXPERIMENTAL PROCEDURES

Chelatable Zinc Fluorescence Microscopy and Spectrofluorometric Quantification—For confocal microscopy, we used the membrane-permeable fluorescent dyes, FluoZin-3^{TM} (K_d ~15 nM; excitation = 494 nm, emission = 516 nm) and Newport Green^{TM} DCF (K_d ~1 μM; excitation = 505 nm, emission = 535 nm) (Invitrogen). A membrane-impermeable FluoZin-3 was used as negative control. For relative fluorescence quantification, we measured chelatable Zn^{2+} levels with a BioTek Synergy 2 spectrofluorometer using the fluorochrome *N*-(6-methoxy-8-quinolyl)-*p*-toluene sulfonamide (TSQ, K_d ~10 nM; excitation = 380 nm, emission = 495 nm) that strongly fluoresces when bound by Zn^{2+} (25). All three fluorescent dyes used in the study are chelatable Zn^{2+}-specific and have low affinity for abundant metals such as calcium and magnesium ions (26, 27).

RNA Interference (RNAi)—We validated the effect of a short hairpin RNA vector targeting human mucolipin-1 gene (TRPML1 shRNA-1208) as described previously (28, 29) and human mucolipin-2 (TRPML2) gene (supplemental Fig. S1). A scrambled shRNA vector control (OriGene Technologies) was also tested and validated (supplemental Fig. S1). Human embryonic kidney (HEK)-293 cells were transfected with TRPML1 and -2 and scrambled shRNA vectors (2 μg) and processed for confocal or electron microscopy (EM) 48 h after transfection. Standard EM technique was performed on TRPML1 RNAi-treated and untreated cells as described (30). For confocal microscopy, the cells were washed with phosphate-buffered saline (PBS), incubated for 30–60 min with either FluoZin-3 or Newport Green DCF (1 μM; Invitrogen) to detect chelatable Zn^{2+}, and incubated with either LysoTracker^{TM} Red DND-99 or Blue DND-22 (0.5 nM; Invitrogen) to detect lysosomes or acidic compartments. LysoTracker Blue DND-22 was used in experiments using TRPML2 and scrambled control shRNA because both plasmids were tagged with a red fluorescent protein marker to monitor expression. The cells were then washed twice with PBS, mounted on slides with ProLong^{TM} Gold antifade reagent (Invitrogen), and imaged without fixation. The red channel was used to show the LysoTracker Blue DND-22 micrographs of TRPML2 RNAi and scrambled RNAi. In other experiments, DAPI was added to stain the cell nucleus.

Primary Cultures of MLIV and Control Fibroblasts—Two MLIV patient skin fibroblast cells (GM 02048 and GM 02527) and two control skin fibroblast cells (GM 00408 and GM 03440) were purchased from Coriell Cell Repositories (Camden, NJ) and cultured in triplicates according to their recommendations. The cells were washed twice with PBS, incubated with TSQ (1 mM) for 30–60 min, washed twice with PBS, and assayed using a BioTek Synergy 2 spectrofluorometer. The relative fluorescence units obtained from Zn^{2+}-TSQ chelates were normalized by total cell numbers per trial using the Cell TiterGlo® viability luminescence kit (Promega) to control for any assay variations.

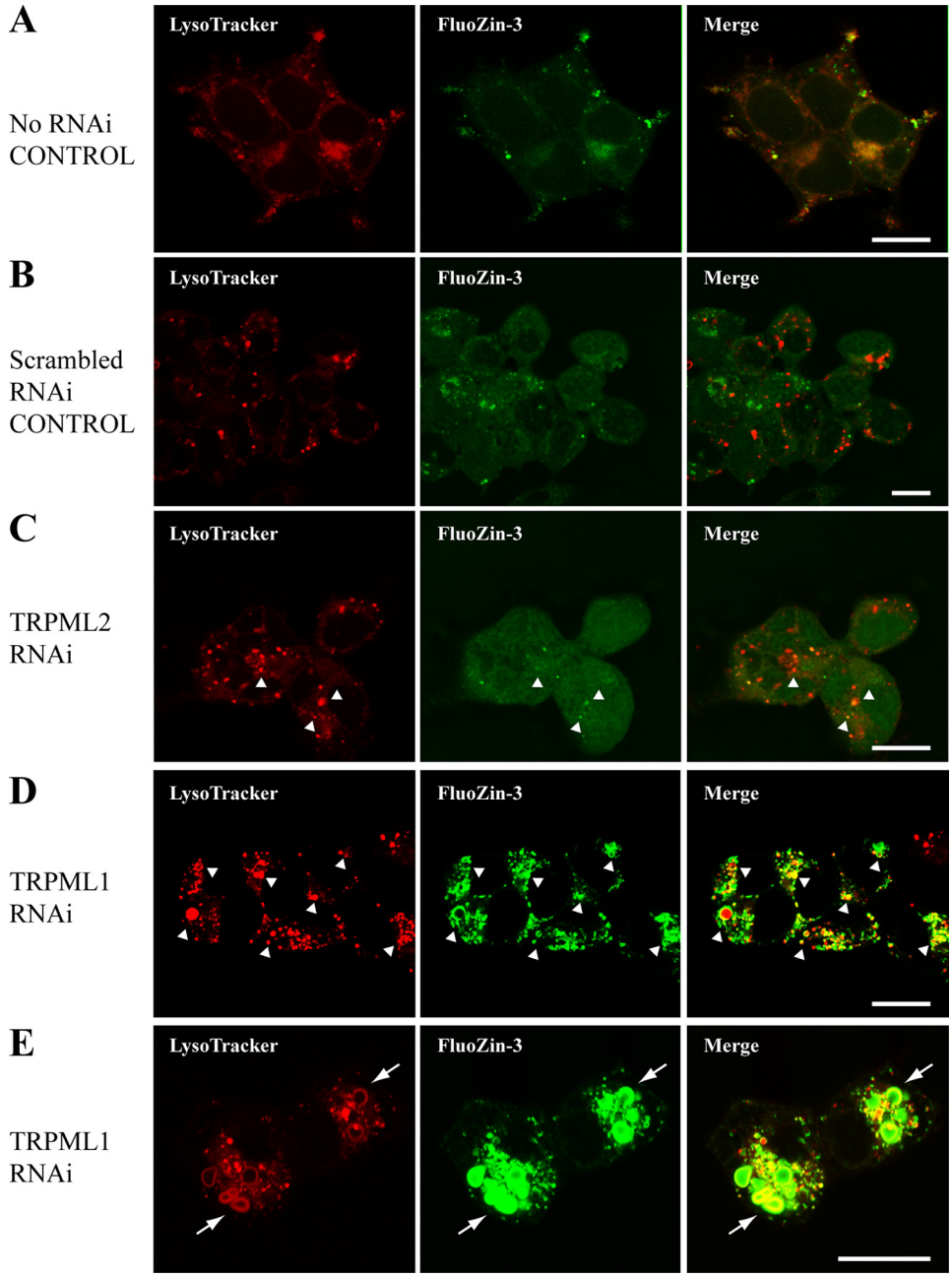

FIGURE 2. **Representative confocal micrographs of control and RNAi-treated HEK-293 cells stained with LysoTracker for lysosomes and FluoZin-3 for chelatable Zn^{2+}.** *A*, untreated control. *B*, scrambled RNAi-treated control. *C*, TRPML2 RNAi-treated cells. *D* and *E*, TRPML1 RNAi-treated cells. In *A* and *B*, some lysosomes (*red*) co-fluoresce with chelatable Zn^{2+} (*green*), but lysosomes in these cells are relatively similar in size. In *C*, an occasional increase in the size of lysosomes corresponds with positive FluoZin-3 stain (arrowheads). Note, however, that TRPML1 RNAi-treated cells in *D* and *E* have a relatively greater number of large lysosomes and vacuoles that also exhibit bright FluoZin-3 fluorescence indicative of chelatable Zn^{2+} accumulation (*arrowheads*). Higher magnification in E shows phagophore-like structures fluorescing both red and green (*arrows*) near other vacuolar organelles. The red channel was used to show the LysoTracker Blue DND-22 micrographs of TRPML2 RNAi and scrambled RNAi. *Scale bars* = 10 μm.

Brain Metal Isotope Analysis—We obtained brain tissues (1 gm) from TRPML1$^{-/-}$ knock-out (KO) mice ($n = 4$), and wild-type (WT) littermate controls ($n = 3$). The frozen brain samples were sent to the California State University Long Beach, Institute for Integrated Research, Materials, Environments, and Society (IIRMES) Core facility for inductively coupled plasma mass spectrometry (ICP-MS) analysis of various metal isotopes such as sodium-23, calcium-43, calcium-44, magnesium-24, aluminum-27, chromium-52, manganese-55, iron-54, iron-57, copper-63, copper-65, and zinc-66. The samples were normalized by total protein content prior to ICP-MS analysis to control for any handling errors introduced during ICP-MS analysis. Data are represented as means ± S.E. and analyzed for statistical significance using Student's *t* test (two-tailed, $p < 0.05$).

RESULTS

To model MLIV *in vitro*, we used RNAi to knock down endogenous TRPML1 protein levels in HEK-293 cells. Electron microscopy showed that TRPML1 RNAi exhibited electron-dense, large membranous vacuoles that were characteristic of MLIV cell phenotype (Fig. 1*A*). RNAi knockdown of cells that normally express TRPML1 has been reported to produce such cell phenotype by 48–72 h (21, 31). Interestingly, phagophore-like membrane structures were also apparent near dense vacuolar structures (horseshoe or half-circle shapes, Fig. 1*A*, *arrows*); phagophores are double membrane structures that initiate autophagy. Fluorescence microscopy showed that lysosomes in these TRPML1 RNAi-treated cells were more pronounced and much larger in comparison with those of untreated control cells (Fig. 1*B*). Indeed, both non-RNAi-treated control and scrambled RNAi-treated control cells had mostly smaller lysosomes with sporadic FluoZin-3 positive Zn^{2+} fluorescence (Fig. 2, *A* and *B*), or Newport Green DCF (supplemental Fig. S2). The TRPML2 RNAi-treated cells occasionally had large LysoTracker-positive lysosomes that co-fluoresced with FluoZin-3 (Fig. 2*C*). However, the size of the lysosomes in these TRPML2 RNAi-treated cells appeared similar to untreated and scrambled RNAi control cells, whereas in TRPML1 RNAi-treated cells, both lysosomes and vacuolar structures that were positive for LysoTracker were brightly fluorescent for chelatable Zn^{2+} as evidenced by either FluoZin-3 (Fig. 2, *D* and *E*) or Newport Green DCF stain (supplemental Fig. S2). No fluorescence was observed using the non-permeable FluoZin-3 control dye (not shown). Noteworthy is a phagophore-like structure that can be

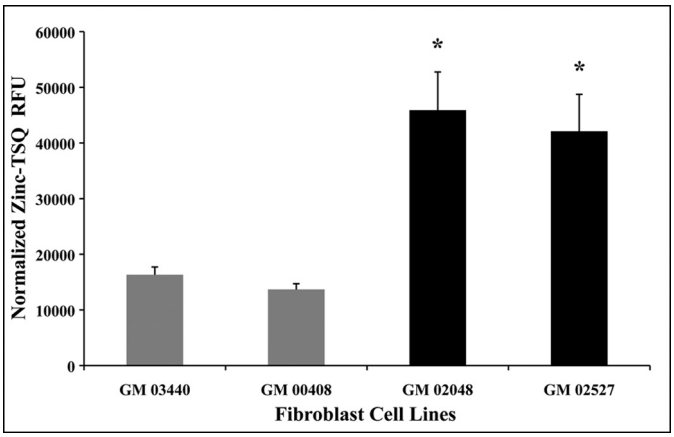

FIGURE 3. **Spectrofluorometric analysis of intracellular chelatable zinc concentrations in cultured MLIV patient skin fibroblasts and control cells.** Normalized relative fluorescence units (*RFU*) of Zn^{2+}-TSQ signals from MLIV fibroblast lines (GM 02048 and GM 02527, *black bars*) are significantly higher than control fibroblast lines (GM 03440 and GM 00408, *gray bars*). This result shows that chelatable zinc levels are elevated in MLIV cells and that chelatable zinc dyshomeostasis is directly associated with the loss of TRPML1 function. Data are represented as means ± S.E., $n = 4$ independent trials, *, $p < 0.05$, Student's *t* test, two-tailed analysis.

seen from TRPML1 RNAi-treated cells co-fluorescing with LysoTracker and FluoZin-3 (Fig. 2*E*).

To determine whether chelatable Zn^{2+} levels were abnormal in TRPML1 RNAi-treated HEK-293 cells when compared with controls, we performed TSQ spectrofluorometric analysis of the samples. We observed an increase of relative Zn^{2+}-TSQ fluorescence in TRPML1 RNAi-treated cells but not with untreated, scrambled RNAi, and TRPML2 RNAi controls (not shown). To verify whether this observation was relevant within the context of MLIV pathology, we quantified chelatable Zn^{2+} concentrations in primary cultured MLIV skin fibroblast and non-patient control cells. Spectrofluorometric quantification revealed a significant 2–3-fold increase in relative Zn^{2+}-TSQ fluorescence in fibroblasts of MLIV patients (GM 02048 and GM 02527) when compared with control fibroblast cells (GM 03440 and GM 00408) (Fig. 3). Because neurons are affected by MLIV, our *in vitro* findings prompted us to further study Zn^{2+} levels using whole brain tissues of TRPML1$^{-/-}$ KO mice and WT littermates. Indeed, ICP-MS analysis showed a small but significant increase in the concentration of zinc isotope-66 (^{66}Zn) from TRPML1$^{-/-}$ KO mouse brain tissues (11.16 ± 0.5 μg/g; $p < 0.05$) but not from WT littermate controls (9.34 ± 0.4 μg/g). No other metal isotopes analyzed were found to be significantly different in these samples (not shown).

DISCUSSION

Our study shows that the loss of TRPML1 function leads to significant accumulation of chelatable Zn^{2+} in large lysosomes and vacuolar structures. Chelatable Zn^{2+} fluorescence is observed within lysosomal lumen and vacuolar lumen. These results intriguingly resemble what has been reported as a Zn^{2+} buildup in ethambutol-induced vacuoles in retinal cells (13, 14) and hydrogen peroxide-induced autophagic vacuoles in astrocytes (12). Chelatable Zn^{2+} appears to mediate autophagic and lysosomal vacuole formation in these aforementioned cells because Zn^{2+} chelation reduces such an effect, but whether it could also be involved in vacuolar formation upon the loss of TRPML1 function remains to be determined. Nevertheless, significant chelatable Zn^{2+} elevation was evident in MLIV patient fibroblast cells, as well as in the whole brain tissue of TRPML1$^{-/-}$ KO mice. It would have been ideal to study the levels of zinc using human postmortem MLIV brain tissue in addition to the mouse model, but unfortunately, such precious tissue was not available for our investigation.

We found a 2–3-fold increase in chelatable Zn^{2+} levels using spectrofluorometry, whereas our ICP-MS data showed a modest increase in ^{66}Zn isotope levels. The difference in magnitude can be explained by methodological differences; the former measured chelatable levels, whereas the latter measured total tissue zinc isotope contents. Moreover, diet and drinking water in rodents have been shown to influence brain zinc levels (32, 33), making whole brain tissue analysis of trace metals from rodents more prone to variability in comparison with cultured cells where known amounts of trace metals are found in media or buffers. Nevertheless, we clearly established that abnormal Zn^{2+} metabolism is present in MLIV cells. Specifically, the loss of TRPML1 appears to increase the amount of chelatable Zn^{2+} in the lysosomes but not in untreated control, scrambled RNAi-treated, and TRPML2 RNAi-treated cells. Although RNAi-mediated TRPML2 knockdown has been previously shown to exhibit similar EM-dense membranous structure in HeLa cells (31), our results showed only a few large lysosomes that also co-localized with chelatable Zn^{2+} fluorescence despite the fact that the TRPML2 shRNA vector efficiently knocked down heterologously overexpressed TRPML2 protein. This observation suggests that the loss or disruption of TRPML1 protein function makes cells highly vulnerable to intracellular chelatable Zn^{2+} dyshomeostasis.

Recently, histochemical evidence using Prussian blue stain showed that chelatable Fe^{2+} levels in the cytosol were reduced, whereas its levels in lysosomes were elevated in MLIV fibroblast cells with distinct mucolipin-1 gene mutation (22). However, we did not observe a significant change in iron isotope levels from TRPML1$^{-/-}$ KO mouse brain samples, but rather found that ^{66}Zn levels were significantly different. Furthermore, colorimetric measurement of total Fe^{2+} levels in TRPML1 RNAi-treated HEK-293 cells did not show significant changes when compared with untreated control.[4] It is possible that differences in the techniques may explain such discrepancies; the previous study looked at chelatable Fe^{2+} concentrations in MLIV fibroblast using Prussian blue stain (22), whereas our collaborators[4] quantified total Fe^{2+} concentrations of TRPML1 RNAi-treated cultured cells using the wet-ash method, and we quantified levels of iron isotopes from TRPML1$^{-/-}$ KO mice using ICP-MS.

The known cellular and mitochondrial toxicities of chelatable Zn^{2+} (1, 6, 7) suggest that our findings could be relevant to cell death and progressive degeneration in MLIV. Likewise, high levels of dietary zinc have been shown to induce iron deficiency and anemia in rodents (34). Because anemia is a clinical feature of MLIV, it would be interesting to know whether

[4] C. Morrison and M. Linder, personal communication.

changes in systemic and/or tissue zinc levels of MLIV patients correlate with iron deficiency and anemia.

In conclusion, we showed for the first time that Zn^{2+} metabolism is impaired in cells lacking a functional TRPML1 ion channel. These findings support our hypothesis that TRPML1 dysfunction leads to changes in concentrations of chelatable Zn^{2+} pool, but not Fe^{2+}, as evidenced by both cellular and *in vivo* models of MLIV disease. Future research should investigate whether chelatable Zn^{2+} elevation contributes to cell death and progressive degeneration of neuronal and retinal cells using the mouse model for MLIV and whether the use of zinc-specific chelator could reverse such negative effects.

Acknowledgments—We are grateful for the technical support given by Karn Sorasaenee, Steve Karl, Mohammad Samie, and Katrina Taylor. We also thank Dr. Maria Linder for help and technical advice in iron analysis. We also thank Dr. Maria Linder and Dr. Sean Murray for critiquing the manuscript.

REFERENCES

1. Cuajungco, M. P., and Lees, G. J. (1997) *Neurobiol. Dis.* **4,** 137–169
2. Frederickson, C. J., Koh, J. Y., and Bush, A. I. (2005) *Nat. Rev. Neurosci.* **6,** 449–462
3. Frederickson, C. J. (1989) *Int. Rev. Neurobiol.* **31,** 145–238
4. Howell, G. A., Welch, M. G., and Frederickson, C. J. (1984) *Nature* **308,** 736–738
5. Cuajungco, M. P., and Lees, G. J. (1998) *Brain Res.* **799,** 118–129
6. Choi, D. W., Yokoyama, M., and Koh, J. (1988) *Neuroscience* **24,** 67–79
7. Sensi, S. L., Ton-That, D., Sullivan, P. G., Jonas, E. A., Gee, K. R., Kaczmarek, L. K., and Weiss, J. H. (2003) *Proc. Natl. Acad. Sci. U.S.A.* **100,** 6157–6162
8. Choi, D. W., and Koh, J. Y. (1998) *Annu. Rev. Neurosci.* **21,** 347–375
9. Sensi, S. L., Canzoniero, L. M., Yu, S. P., Ying, H. S., Koh, J. Y., Kerchner, G. A., and Choi, D. W. (1997) *J. Neurosci.* **17,** 9554–9564
10. Falcón-Pérez, J. M., and Dell'Angelica, E. C. (2007) *Exp. Cell Res.* **313,** 1473–1483
11. Hwang, J. J., Lee, S. J., Kim, T. Y., Cho, J. H., and Koh, J. Y. (2008) *J. Neurosci.* **28,** 3114–3122
12. Lee, S. J., Cho, K. S., and Koh, J. Y. (2009) *Glia* **57,** 1351–1361
13. Chung, H., Yoon, Y. H., Hwang, J. J., Cho, K. S., Koh, J. Y., and Kim, J. G. (2009) *Toxicol. Appl. Pharmacol.* **235,** 163–170
14. Yoon, Y. H., Jung, K. H., Sadun, A. A., Shin, H. C., and Koh, J. Y. (2000) *Toxicol. Appl. Pharmacol.* **162,** 107–114
15. Jennings, J. J., Jr., Zhu, J. H., Rbaibi, Y., Luo, X., Chu, C. T., and Kiselyov, K. (2006) *J. Biol. Chem.* **281,** 39041–39050
16. Soyombo, A. A., Tjon-Kon-Sang, S., Rbaibi, Y., Bashllari, E., Bisceglia, J., Muallem, S., and Kiselyov, K. (2006) *J. Biol. Chem.* **281,** 7294–7301
17. Venugopal, B., Mesires, N. T., Kennedy, J. C., Curcio-Morelli, C., Laplante, J. M., Dice, J. F., and Slaugenhaupt, S. A. (2009) *J. Cell. Physiol.* **219,** 344–353
18. Vergarajauregui, S., Connelly, P. S., Daniels, M. P., and Puertollano, R. (2008) *Hum. Mol. Genet.* **17,** 2723–2737
19. Amir, N., Zlotogora, J., and Bach, G. (1987) *Pediatrics* **79,** 953–959
20. Kogot-Levin, A., Zeigler, M., Ornoy, A., and Bach, G. (2009) *Pediatr. Res.* **65,** 686–690
21. Miedel, M. T., Rbaibi, Y., Guerriero, C. J., Colletti, G., Weixel, K. M., Weisz, O. A., and Kiselyov, K. (2008) *J. Exp. Med.* **205,** 1477–1490
22. Dong, X. P., Cheng, X., Mills, E., Delling, M., Wang, F., Kurz, T., and Xu, H. (2008) *Nature* **455,** 992–996
23. Grimm, C., Cuajungco, M. P., van Aken, A. F., Schnee, M., Jörs, S., Kros, C. J., Ricci, A. J., and Heller, S. (2007) *Proc. Natl. Acad. Sci. U.S.A.* **104,** 19583–19588
24. Xu, H., Delling, M., Li, L., Dong, X., and Clapham, D. E. (2007) *Proc. Natl. Acad. Sci. U.S.A.* **104,** 18321–18326
25. Frederickson, C. J., Kasarskis, E. J., Ringo, D., and Frederickson, R. E. (1987) *J. Neurosci. Methods* **20,** 91–103
26. Gee, K. R., Zhou, Z. L., Ton-That, D., Sensi, S. L., and Weiss, J. H. (2002) *Cell Calcium* **31,** 245–251
27. Jiang, P., and Guo, Z. (2004) *Coord. Chem. Rev.* **248,** 205–229
28. Grimm, C., Jörs, S., Saldanha, S. A., Obukhov, A. G., Pan, B., Oshima, K., Cuajungco, M. P., Chase, P., Hodder, P., and Heller, S. (2010) *Chem. Biol.* **17,** 135–148
29. Samie, M. A., Grimm, C., Evans, J. A., Curcio-Morelli, C., Heller, S., Slaugenhaupt, S. A., and Cuajungco, M. P. (2009) *Pflugers Arch* **459,** 79–91
30. Hirose, K., Westrum, L. E., Cunningham, D. E., and Rubel, E. W. (2004) *J. Comp. Neurol.* **470,** 164–180
31. Zeevi, D. A., Frumkin, A., Offen-Glasner, V., Kogot-Levin, A., and Bach, G. (2009) *J. Pathol.* **219,** 153–162
32. Flinn, J. M., Hunter, D., Linkous, D. H., Lanzirotti, A., Smith, L. N., Brightwell, J., and Jones, B. F. (2005) *Physiol. Behav.* **83,** 793–803
33. Linkous, D. H., Adlard, P. A., Wanschura, P. B., Conko, K. M., and Flinn, J. M. (2009) *J. Alzheimers Dis.* **18,** 565–579
34. Yanagisawa, H., Miyakoshi, Y., Kobayashi, K., Sakae, K., Kawasaki, I., Suzuki, Y., and Tamura, J. (2009) *Toxicol. Lett.* **191,** 15–19